Additions to the Spectrum of Fe IX in the 110–200 Å Region

Alexander N. Ryabtsev[1] , Edward Y. Kononov[1], and Peter R. Young[2,3]
[1] Institute of Spectroscopy, Russian Academy of Sciences, Troitsk, Moscow 108840, Russia
[2] NASA Goddard Space Flight Center, Greenbelt, MD 20771, USA
[3] Northumbria University, Newcastle upon Tyne, NE1 8ST, UK; peter.r.young@nasa.gov

Abstract

The spectrum of eight-times ionized iron, Fe IX, was studied in the 110–200 Å region. A low inductance vacuum spark and a 3 m grazing incidence spectrograph were used for the excitation and recording of the spectrum. Previous analyses of Fe IX have been greatly extended and partly revised. The number of known lines in the $3p^53d–3p^54f$ and $3p^53d–3p^43d^2$ transition arrays is extended to 25 and 81, respectively. Most of the identifications of the Fe IX lines from the $3p^53d–3p^43d^2$ transition array in the solar spectrum have been confirmed and several new identifications are suggested.

Unified Astronomy Thesaurus concepts: Atomic spectroscopy (2099); Spectroscopy (1558); Line intensities (2084); Solar extreme ultraviolet emission (1493); Solar atmosphere (1477)

1. Introduction

Eight-times ionized iron, Fe IX, belongs to the argon isoelectronic sequence with a fully occupied $3p^6$ ground configuration. The strongest line in the Fe IX spectrum is the $3p^6\ ^1S_0–3p^53d\ ^1P_1$ resonance transition at 171.073 Å, which was identified independently by Gabriel & Fawcett (1965) and Alexander et al. (1965). The reference wavelength for the line listed in the NIST database (Kramida et al. 2021) comes from the solar spectral atlas of Behring et al. (1972). In the past four decades, the 171 Å line has been a popular choice for solar extreme ultraviolet (EUV) imaging instruments on account of its strength, relative isolation in the spectrum, and the proximity of an aluminum absorption edge at 170 Å. EUV imaging instruments make use of multilayer coatings to yield narrow bandpasses that are typically 10% of the central wavelength. However, the high density of lines in the EUV means that multiple strong lines can contribute to the imaging channel emission. Aluminum filters are used to block visible radiation in these instruments, and the aluminum edge at 170 Å strongly attenuates emission to the short-wavelength side of Fe IX 171.07 Å, yielding a relatively clean bandpass. Because of this, a filter at or close to 171 Å has been used for several telescopes on spacecraft, including the EUV Imaging Telescope (EIT; Delaboudinière et al. 1995), the Transition Region and Coronal Explorer (TRACE; Handy et al. 1999), the Extreme Ultraviolet Imager (EUVI; Howard et al. 2008), the Atmospheric Imaging Assembly (AIA; Lemen et al. 2012), and most recently the Extreme Ultraviolet Imager (EUI; Rochus et al. 2020) on Solar Orbiter. The 171.07 Å line has also been measured in spectra of the cool stars Procyon (Drake et al. 1995) and α Centauri (Drake et al. 1997).

Other Fe IX lines in the EUV are much weaker, but the ratio of the lines at 241.74 and 244.91 Å (decays from the $3p^53d\ ^3P_{2,1}$ states to the ground) has long been recognized as a useful density diagnostic of the solar atmosphere (Feldman et al. 1978).

The first excited configuration of Fe IX, $3s^23p^53d$, has 12 fine-structure levels and yields a rich spectrum of forbidden lines between 1738 Å and 2.9 μm. Many of these lines have been measured during solar eclipses, and a summary is provided by Del Zanna & DeLuca (2018).

At soft X-ray wavelengths, there are three groups of lines coming from $n = 4$ configurations. The $3p^6–3p^54d$ and $3p^6–3p^54s$ transition arrays give two pairs of lines at 82.43 and 83.46 Å, and 103.57 and 105.21 Å, respectively, and these lines were reported in a solar spectrum by Malinovsky & Heroux (1973). The $3p^53d–3p^54f$ array gives a group of lines between 111 and 120 Å and an additional pair of lines at 133.92 and 136.57 Å. None of these lines have been reported from solar spectra, but they have been studied with laboratory spectra. This array is the subject of study in the present article and is discussed in Section 3.1.

Recent advances in the spectral analysis of Fe IX have largely been motivated by the solar spectra obtained with the EUV Imaging Spectrometer (EIS: Culhane et al. 2007) on board the Hinode spacecraft, launched in 2006. EIS has a spectral resolution of 3000 and it covers the wavelength ranges 170–212 Å and 246–292 Å, which contain a wealth of emission lines from iron ions, ranging from Fe VII up to Fe XXIV (Young et al. 2007). Brown et al. (2008) reported that about half of the lines in the EIS wavelength ranges were unidentified. Young (2009) was the first to report new Fe IX identifications in the EIS wavelength bands, and further studies of the Fe IX spectrum have been performed by Del Zanna (2009), Landi & Young (2009a, 2009b), Young & Landi (2009), O'Dwyer et al. (2012), and Del Zanna et al. (2014). Laboratory studies of the Fe IX spectrum in the EUV have been performed by Liang et al. (2009), Beiersdorfer & Lepson (2012), and Beiersdorfer & Träbert (2018). These works have resulted in a number of line identifications from the $3p^53d–3p^43d^2$ transitions and around two dozen lines suggested as due to Fe IX but without definite identifications.

The present work focuses on line identifications in the 110–200 Å range from the $3p^53d–3p^54f$ and $3p^53d–3p^43d^2$ transition arrays. Figure 1 gives an overview of the known (prior to the present work) Fe IX transitions in the 100–220 Å as found in version 10 of the CHIANTI atomic database (Young et al. 2016;
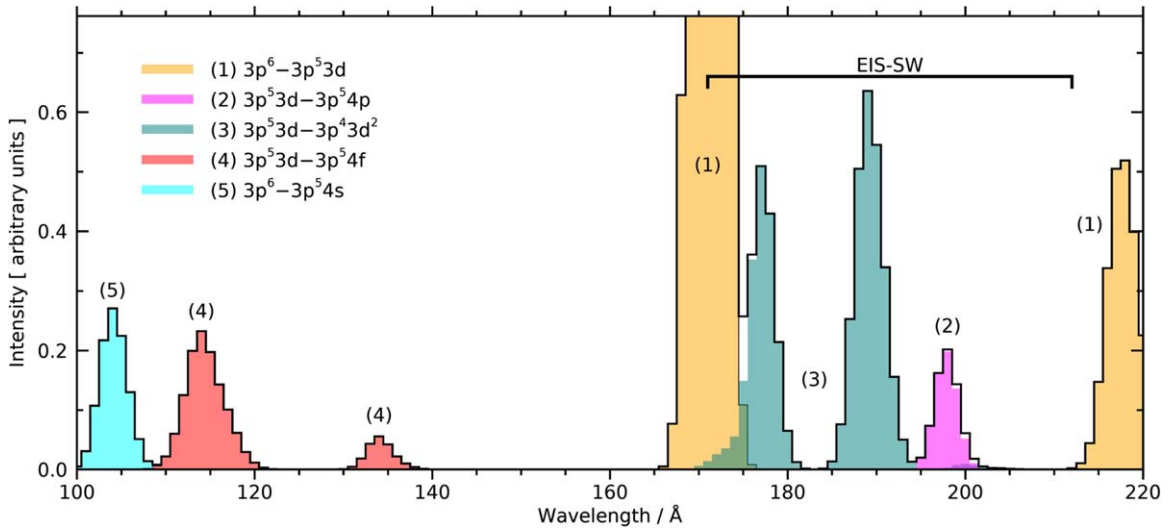
Figure 1. A CHIANTI synthetic spectrum showing the location of known Fe IX lines. Colors and numbers denote different transition arrays. Line profiles are represented as Gaussians with an FWHM of 3 Å. A temperature of 0.8 MK and an electron number density of 4.0×10^8 cm^{-3} were used. The wavelength range of the EIS short-wavelength (SW) band is indicated.

Del Zanna et al. 2021). The spectrum was generated using a temperature of 0.8 MK and an electron number density of 4.0×10^8 cm^{-3}, which are typical of conditions in the solar atmosphere. Emission line widths have been set to 3 Å in order to group nearby lines together. Five transition arrays are highlighted: the two studied in this work, and the $3p^6$–$3p^54s$, $3p^53d$–$3p^54p$, and $3p^6$–$3p^53d$ arrays. The latter yields the 171 Å line, which towers over the other features to an intensity peak of 10 on the plot scale. The only known line from the $3p^53d$–$3p^54p$ array is at 197.86 Å (Young 2009). Note that there are many more transitions in CHIANTI in this part of the spectrum that are not shown because they only have theoretical wavelengths.

Our new laboratory study uses spectra excited in a vacuum spark and recorded with a higher resolution than in all previous papers. The number of known lines in the $3p^53d$–$3p^54f$ transition array is extended to 25. Several previous identifications were corrected resulting in changes to the energies of the corresponding levels. Eighty-one lines of the $3p^53d$–$3p^43d^2$ array have been identified. Most of the previous identifications from this array in the solar spectrum have been confirmed and several new ones have been made. Lines previously assigned to Fe IX but not identified have been classified. This article continues a series of publications on laboratory high-resolution studies of iron ion spectra (Ryabtsev 2017; Young et al. 2021; Kramida et al. 2022) relevant for diagnostics of solar plasma.

Section 2 describes the experimental setup used to obtain the Fe IX spectra. Section 3 gives the line identification results for the two transition arrays, and we give our conclusions in Section 4.

2. Experiment

The procedures used in our earlier studies of the iron ions (see, for example, Kramida et al. 2022) were followed in the present measurements. In short, the spectra were taken with a 3 m grazing incidence (5°) spectrograph equipped with a 3600 line mm^{-1} grating. The spectra were excited in a three-electrode vacuum spark run with peak currents up to 100 kA. The high current tracks on the ORWO UV-2 photographic plates taken for analysis of Fe VIII (Ramonas & Ryabtsev 1980) were measured. The tracks were scanned on an EPSON

EXPRESSION scanner and then digitized and measured using the Gfit code (Engström 1998).

Spectra were also recorded on phosphor imaging plates (Fuji BAS-TR) (Ryabtsev 2017). These spectra were scanned using a 0.01 mm scanning step with a Typhoon FLA 9500 reader and processed and analyzed with the ImageQuant TL 7.0 image analysis software. For the final reduction of the spectra, the GFit code again was employed. Because of a high level of background, the imaging plate spectra taken at high currents were useful only for wavelengths above around 140 Å.

Figure 2 shows the photoplate spectrum between 110 and 140 Å obtained for a current of 40 kA, and Figures 3 and 4 show the photoplate spectrum between 140 and 201 Å obtained at 100 kA. The wavelength scales are not the final ones used to derive the Fe IX wavelengths as a grating formula with averaged parameters was used. The final Fe IX wavelengths, given in Tables 1 and 3, were obtained following a reduction with reference lines and a correction curve of the photoplate. Close-ups of selected portions of the spectra are shown in Figures 5–7, where spectra obtained for different currents are compared.

The iron line wavelengths were measured by first taking photoplate spectra with an iron anode and a titanium cathode of the spark, giving a mixed spectrum of iron and titanium lines. The known titanium wavelengths (Svensson 1969) were used to derive reference wavelengths for those iron lines that are not blended with titanium lines. These iron line wavelengths were then used as secondary standards when reducing the pure iron spectra obtained with both iron electrodes in the vacuum spark. The width of the Fe IX lines on the photoplate spectra in the region above 140 Å was about 0.03 Å whereas on the imaging plate spectra the width was larger by about 20%. The photoplate containing the spectrum below 140 Å that was used for the analysis of the $3p^53d$–$3p^54f$ transitions had a better resolution, with line widths around 0.02 Å. The photoplate spectra possessed two other advantages with respect to the imaging plate spectra that were important for the wavelength measurements. First, the signal to noise was better due to a smaller background, and second, the line shape was smoother due to the approximately two times smaller scanning step of the
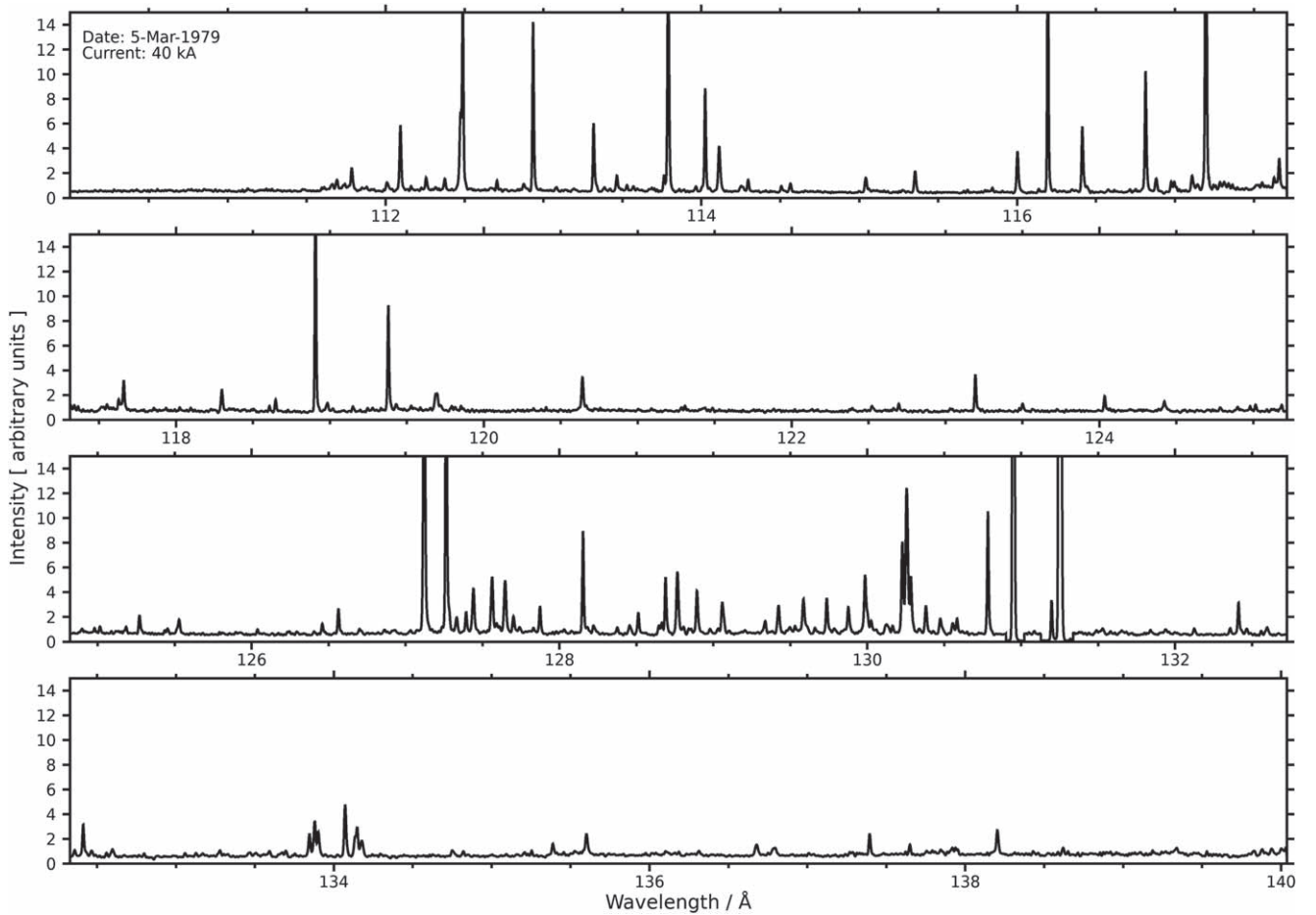
Figure 2. The photoplate spectrum obtained at a current of 40 kA.

EPSON EXPRESSION scanner in comparison with the Typhoon FLA 9500 reader. The rms deviation of the reference titanium, as well as the secondary iron, lines from the calibration curve was 0.002 Å, and the deviations from the mean values of the wavelengths obtained from the measurements of different spectra recordings were below 0.001 Å. Because Svensson (1969) claimed an uncertainty of 0.004 Å for their wavelengths we adopt this value as our wavelength uncertainty for single, unperturbed lines. This estimation is supported by the deviations of the measured wavelengths from the Ritz values calculated in the present spectrum analysis. Where possible, the line intensities were obtained from the imaging plate spectra due to the greater linearity of the response. The intensities will be given on an arbitrary scale without taking into account the wavelength dependence of the spectrograph efficiency and recording media sensitivity.

Based on our past experience with the vacuum spark, the plasma is in approximate local thermodynamic equilibrium with an effective electron temperature. Rough estimates following the procedure of Kramida et al. (2022) for Fe VII give a value of 10 eV. It is not possible to estimate a density from the spectra, but we expect a value around $10^{17}\,\mathrm{cm}^{-3}$ based on measurements from similar plasma discharges. The density would be expected to vary as the current is varied to modify the charge balance.

The Fe IX analysis was guided by calculations with the Cowan atomic code (Cowan 1981; Kramida 2019). The set of even parity configurations used was $3p^6$, $3p^5np$ ($n = 4$–6),

$3p^5nf$ ($n = 4$–6), $3p^43d^2$, $3p^44s^2$, $3p^43d4s$, $3p^44d4s$, $3s3p^63d$, and $3s3p^64s$. The set of interacting odd parity configurations was restricted to $3p^5nd$ ($n = 3$–6), $3p^54s$, $3p^55s$, $3s3p^64p$, and $3s3p^64f$. The calculated energy levels and transition probabilities were used as input to the IDEN2 line identification code (Azarov et al. 2018).

3. Results

3.1. The $3p^53d$–$3p^54f$ Transitions

Laboratory measurements of the $3p^53d$–$3p^54f$ transition array were performed in the 1970s, with Wagner & House (1971) listing 12 lines in the 111–117 Å range. Nine of these were measured by Fawcett et al. (1972) with an accuracy of ± 0.01 Å, and further work was done by Swartz et al. (1976) who remeasured all 12 lines, yielding energies for 10 of the 12 $3p^54f$ levels with an estimated uncertainty of $\pm 200\,\mathrm{cm}^{-1}$.

More recently, O'Dwyer et al. (2012) provided a list of 20 identified $3p^53d$–$3p^54f$ lines and all level energies of the $3p^54f$ configuration. The wavelengths include the 11 values from Fawcett et al. (1972), but the source of the other nine wavelengths is not given. We speculate that the authors had access to the original plate of Fawcett and performed new measurements as done in the earlier works of Del Zanna (2009) and Del Zanna (2012). O'Dwyer et al. (2012) did not provide uncertainties on their derived level energies.

Our results for this transition array are displayed in Table 1 for the wavelengths and in Table 2 for the energy levels of the
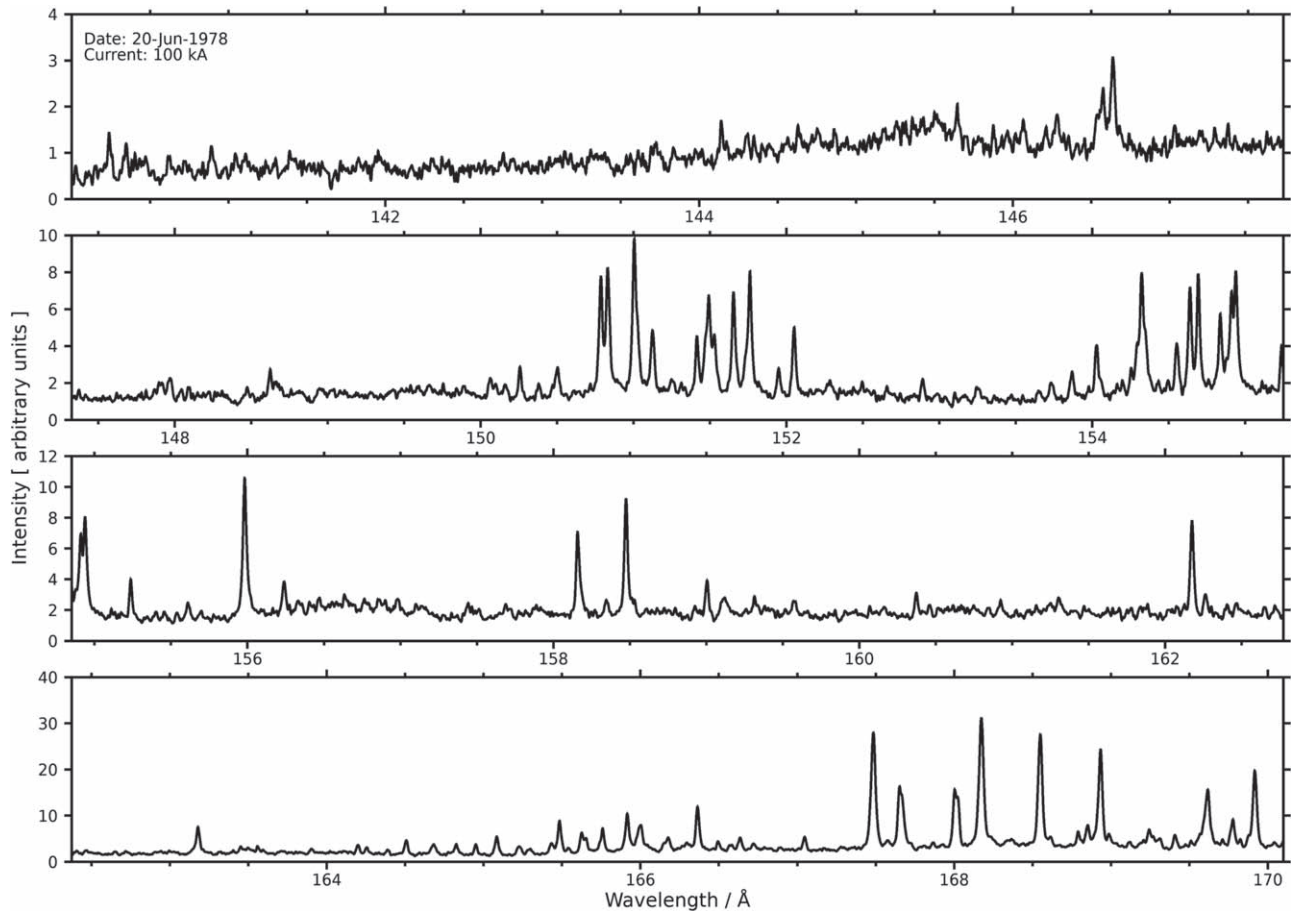
Figure 3. A section of the photoplate spectrum obtained at a current of 100 kA.

$3p^5 4f$ configuration. Many weak lines were added to the previous analyses of these transitions extending to 25 the number of identified lines and resulting in the location of all the $3p^5 4f$ levels with uncertainties $30 \, \text{cm}^{-1}$ or less. The wavelengths of several lines marked by VII in Table 1 are close to the Fe VII wavelengths of Ekberg (1981). Indeed, these lines together with the other Fe VII lines are present in our tracks with *colder* iron spectra but their influence on the intensities and wavelengths of the Fe IX lines is negligible in our case. One line with Ritz value $112.463(3) \, \text{Å}$ is not measured, possibly being masked by the Fe VIII $112.472 \, \text{Å}$ line.

The relative intensities measured in the photographic plate spectrum are given on an arbitrary linear scale. The 250 value was adopted for the strongest line ($113.789 \, \text{Å}$) for convenient comparison with the corresponding gA values. (g is the statistical weight of the transition upper level and A the radiative decay rate.) The wavelength responses of the grating and photoplate were not taken into account. Even for a narrow wavelength range, the intensities should be considered as more qualitative than quantitative because of a possible error in the model characteristic curve of the photoplate used for a transformation of the measured line densities to their intensities.

Table 1 contains a comparison with the previous measurements by Swartz et al. (1976) and O'Dwyer et al. (2012). Good agreement of all measurements with some exceptions is seen. The two lines at 111.713 and $112.031 \, \text{Å}$ were listed by O'Dwyer et al. (2012) as the transitions from the $3p^5 4f \, ^3D_1$ level. A part of the iron spectrum in the region of these lines,

taken at two modes of the spark operation, is shown in Figure 5. Fe IX lines are clearly distinguished from those of Fe VII and Fe VIII by the change in intensity from *cold* to *hot* spark conditions. The Fe IX lines have about the same intensity in the displayed spectra, while the lower ionization states have reduced intensities in the hot spectrum. Both the 111.713 and $112.031 \, \text{Å}$ lines identified by O'Dwyer et al. (2012) are seen to belong to lower ionization states than Fe IX. The feature at $112.031 \, \text{Å}$ is a known line of Fe VII, measured at $112.030 \, \text{Å}$ by Ekberg (1981). The lines at 111.692 and $112.011 \, \text{Å}$ (marked with arrows in Figure 5) show behavior similar to the other Fe IX lines and were adopted as the transitions from the $3p^5 4f$ $^3D_1$ level. The wavelengths are in good agreement with those of Swartz et al. (1976).

The line of $118.27 \, \text{Å}$ identified by Swartz et al. (1976) as the $3p^5 3d \, ^1F_3 - 3p^5 4f \, ^3F_4$ transition has a low transition probability and is absent in our spectrum. Its Ritz value is $118.220(3) \, \text{Å}$.

Previous Fe IX studies did not provide definitive line identifications for the $3p^5 4f \, ^1D_2$ and $3p^5 4f \, ^3F_2$ levels. Swartz et al. tentatively suggested that the two lines at 134.743 and $115.46 \, \text{Å}$ belong to decays from the $3p^5 4f \, ^1D_2$ level to the $3p^5 3d \, ^1P_1$ and $^3D_1$ levels, resulting in a value of $1{,}326{,}700 \, \text{cm}^{-1}$ for the $^1D_2$ level. It should be noted that both lines are not present in our hot spectrum, the second one being possibly the $115.472 \, \text{Å}$ line of Fe VII (Ekberg 1981). Lepson et al. (2002) recorded an Fe IX spectrum at the Lawrence Livermore electron beam ion trap (EBIT). The spectral resolution was relatively low (around 300 at $100 \, \text{Å}$) and the
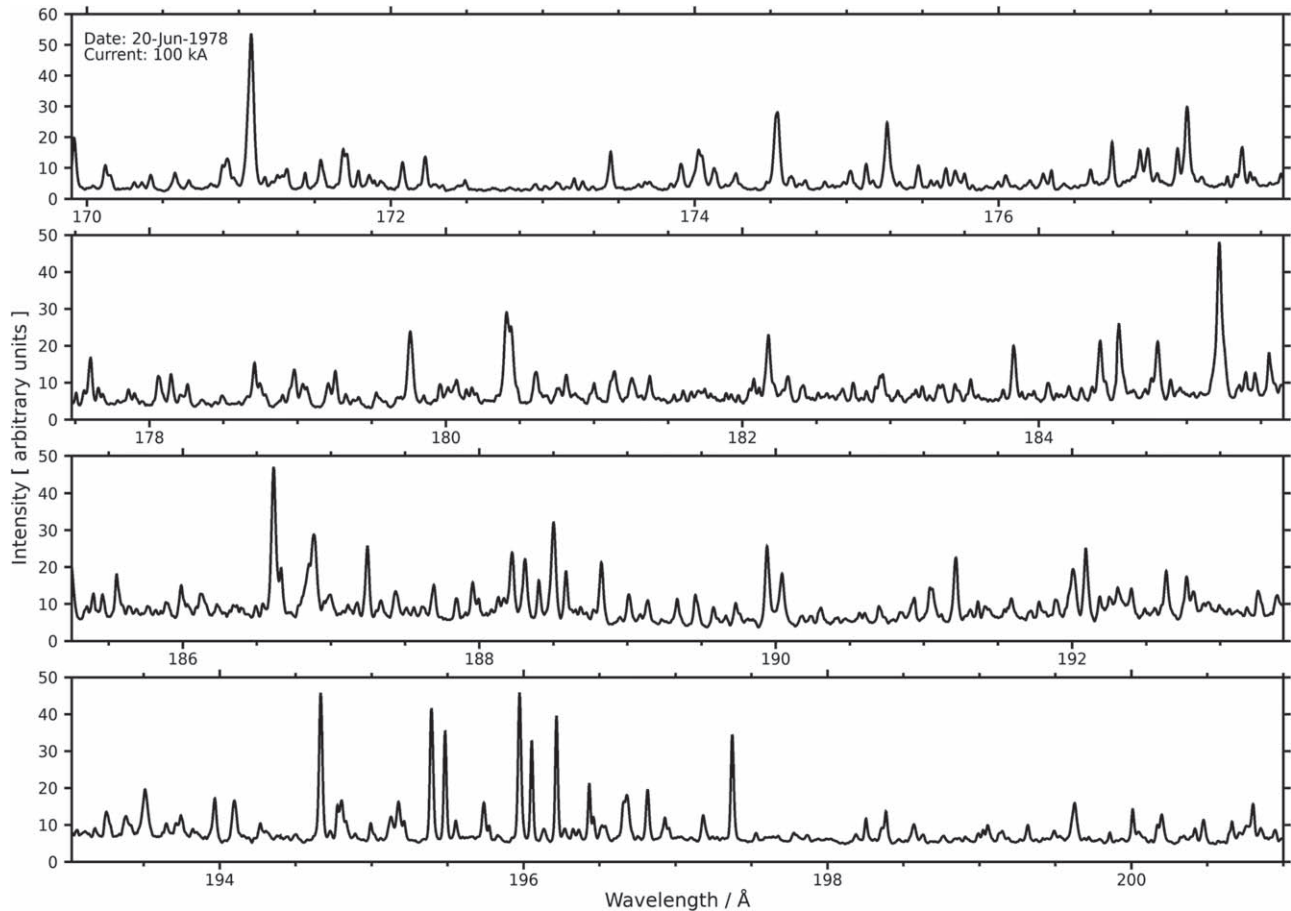
Figure 4. A section of the photoplate spectrum obtained at a current of 100 kA.

authors measured two weak lines at 134.08 and 136.70 Å that they assigned to $3d$–$4f$ transitions, although level assignments were not made. The same lines were identified in low-resolution (around 150 at 130 Å) solar spectra from the Extreme Ultraviolet Variability Experiment (EVE; Woods et al. 2012) by Foster & Testa (2011), although level information was not provided.

Our high-resolution spectra reveal several lines near the location of the Lepson et al. (2002) 134.08 Å line (Figure 6). Of these, the 134.063 and 134.128 Å lines belong to Fe VII (Ekberg 1981), while the 134.169 Å line shows behavior consistent with the Fe IX lines shown in Figure 5. We identify this line with the $3p^53d$ $^1P_1$–$3p^54f$ $^1D_2$ transition, which is supported by the Ritz transition to the $3p^53d$ $^3D_1$ level with a wavelength of 115.042 Å. The energy of the $3p^54f$ $^1D_2$ level of 1,329,872 cm^{-1} is consistent with the energy calculated from the Cowan code. O'Dwyer et al. (2012) suggested the $3p^53d^1P_1$–$3p^54f$ $^1D_2$ transition belonged to a line at 133.923 Å. Our spectra have a line at 133.899 Å that is due to Fe VII (Ekberg 1981). Possibly, this Fe VII line was identified by O'Dwyer et al. (2012) as Fe IX with a measured value of 133.923 Å. It should be noted that the other lines at 114.860 and 115.124 Å attributed by O'Dwyer et al. (2012) to the transitions from the $3p^54f$ $^1D_2$ level are not present in our spectra.

Our value of 136.674 Å for the $3p^53d$ $^1P_1$–$3p^54f$ $^3F_2$ transition is in agreement with the Lepson et al. (2002) measurement. The corresponding energy of 1,316,205 cm^{-1} for the $3p^54f$ $^3F_2$ level is in good agreement with the value computed from the Cowan code. It is also supported by a Ritz combination to the $3p^53d$ $^3D_1$ level. The corresponding line at

116.881 Å was the only remaining line in this region of the spectrum that had the properties of Fe IX. On the other hand, O'Dwyer et al. (2012) attributed a line at 136.572 Å to the $3p^53d$ $^1P_1$–$3p^54f$ $^3F_2$ transition with Ritz support from lines at 113.258 and 116.803 Å. No Fe IX lines can be identified in our hot spectrum at 136.572 and 113.258 Å. The 116.803 Å line, measured in our spectrum at 116.814 Å, is assigned to the $3p^53d$ $^3D_3$–$3p^54f$ $^3F_4$ transition in Fe IX.

The $3p^54f$ level energies in Table 2 were derived from the identified $3p^53d$–$3p^54f$ lines using the program LOPT for least-squares optimization of energy levels (Kramida 2011). The $3p^53d$ levels were fixed to the values of Edlén & Smitt (1978) for the optimization. The uncertainties of our level energies range from 19–40 cm^{-1}. Column 2 shows the deviations of the Cowan code energies from the experimental ones after a fitting of 12 energy levels with four free parameters. The deviations are in good agreement with the estimated level of uncertainties. Good agreement is also seen with the energy values found by Swartz et al. (1976) and O'Dwyer et al. (2012) except for the questionable cases noted earlier. The differences in the energies are within 60 cm^{-1}, which shows that the Swartz et al. (1976) uncertainties of ± 200 cm^{-1} were overestimated.

Table 2 shows the designations of the levels in the LS and JJ couplings. It is seen that the JJ-coupling representation is generally better than the LS one. Nevertheless, in Table 1 we are using the more convenient LS designations because it is possible to give unambiguously the LS names to all levels although in several cases they are associated with the second component of their wave function.

Table 1
Wavelengths of the $3p^5 3d$–$3p^5 4f$ Transitions in Fe IX

I^a	gA^b $(10^{10}\,s^{-1})$	λ^c (Å)							$3p^5 3d$		$3p^5 4f$	
		This Work	Ritz^d	TW–Ritz^e	S76	TW-S76	O'D12	TW–O'D12	Term	E (cm^{-1})	Term	E (cm^{-1})
21	22	111.664	111.665(3)	−0.001	…	…	…	…	$^3F_3$	429,310.9	$^1G_4$	1,324,844
27	35	111.692	111.692(4)	0.000	111.689	0.003	111.713	−0.021	$^3P_0$	405,772	$^3D_1$	1,301,088
51	73	111.785	111.790(3)	−0.005	111.795	−0.01	111.791	−0.006	$^3P_1$	408,315.1	$^3D_2$	1,302,850
24	29	112.011 VII	112.011(4)	0.000	112.017	−0.006	112.031	−0.020	$^3P_1$	408,315.1	$^3D_1$	1,301,088
108	126	112.093	112.096(3)	−0.003	112.097	−0.004	112.096	−0.003	$^3P_2$	413,669.2	$^3D_3$	1,305,762
29	38	112.375	112.380(3)	−0.005	112.375	0	…	…	$^3F_2$	433,818.8	$^3F_3$	1,323,654
…	30	VIII	112.463(3)	…	…	…	112.464	…	$^3P_2$	413,669.2	$^3D_2$	1,302,850
16	18	112.875	112.880(3)	−0.005	…	…	…	…	$^3F_4$	425,809.8	$^3F_4$	1,311,707
20	24	113.529	113.529(4)	0.000	…	…	…	…	$^3F_3$	429,310.9	$^3G_3$	1,310,147
18	15	113.570	113.572(3)	−0.002	…	…	113.571	−0.001	$^3F_4$	425,809.8	$^3G_4$	1,306,305
250	266	113.789	113.789(5)	…	113.792	−0.003	113.793	−0.004	$^3F_4$	425,809.8	$^3G_5$	1,304,630
136	172	114.024	114.026(3)	−0.002	114.027	−0.003	114.024	0	$^3F_3$	429,310.9	$^3G_4$	1,306,305
98	113	114.112	114.113(4)	−0.001	114.116	−0.004	114.111	0.001	$^3F_2$	433,818.8	$^3G_3$	1,310,147
30	12	115.042 VII	115.044(3)	−0.002	…	…	…	…	$^3D_3$	455,612.2	$^1G_4$	1,324,844
30	34	115.042 VII	115.041(3)	0.001	…	…	…	…	$^3D_1$	460,616	$^1D_2$	1,329,872
51	112	115.354	115.353(3)	0.001	115.344	0.01	115.353	0.001	$^1D_2$	456,752.7	$^3F_3$	1,323,654
84	130	116.002	116.002(5)	…	116.001	0.001	115.996	0.006	$^3D_2$	462,616.6	$^1F_3$	1,324,670
101	172	116.414	116.412(3)	0.000	116.408	0.006	116.408	0.006	$^1F_3$	465,828.4	$^1G_4$	1,324,844
10	9	116.578	116.574(3)	0.004	…	…	…	…	$^1F_3$	465,828.4	$^3F_3$	1,323,654
171	171	116.814 VII	116.809(4)	0.005	116.806	0.008	116.803	0.011	$^3D_3$	455,612.2	$^3F_4$	1,311,707
34	57	116.881 VII	116.879(3)	0.002	…	…	…	…	$^3D_1$	460,616	$^3F_2$	1,316,205
25	32	117.629	117.626(4)	0.003	…	…	117.626	0.003	$^3D_3$	455,612.2	$^3D_3$	1,305,762
19	21	118.984	118.980(3)	0.004	…	…	118.978	0.006	$^1F_3$	465,828.4	$^3G_4$	1,306,305
10	11	119.019	119.015(4)	0.004	…	…	…	…	$^3D_2$	462,616.6	$^3D_2$	1,302,850
35	72	134.169	134.169(4)	0.000	134.743?	−0.574	133.923	0.246	$^1P_1$	584,546	$^1D_2$	1,329,872
21	44	136.674 VII	136.676(4)	−0.002	…	…	136.572	0.102	$^1P_1$	584,546	$^3F_2$	1,316,205

Notes.
^{a} Observed relative intensity in arbitrary units (see text).
^{b} Product of upper level weight g and transition probability A calculated with eigenfunctions obtained from the fitting of the calculated to experimental level energies.
^{c} Symbols: VII—line is present in a list of the Fe VII lines reported by Ekberg (1981), and the influence on the intensity and the wavelength of the corresponding Fe IX line is negligible at present excitation conditions; VIII—line is masked by a wing of the Fe VIII line at 112.472 Å. Previous measurements: S76—Swartz et al. (1976); O'D12—O'Dwyer et al. (2012).
^{d} Wavelength derived from the final level energies (Ritz wavelength).
^{e} A blank value for the TW–Ritz difference indicates that the upper level is derived from that line only.

Table 2
Energy Levels of the $3p^5 4f$ Configuration of Fe IX

E^a (cm^{-1})						Designation^c		N^d
TW	o-c^b	S76	TW-S76	O'D12	TW–O'D12	LS	JJ	
1,301,088(23)	24	1,301,070	18	1,300,923?	165	99% $^3D_1$	99% $(3/2, 5/2)_1$	2
1,302,850(30)	−20	1,302,800	50	1,302,841	9	93% $^3D_2$	53% $(3/2, 5/2)_2$	2
1,304,630(30)	50	1,304,595	35	1,304,598	32	99% $^3G_5$	99% $(3/2, 7/2)_5$	1
1,305,762(30)	−38	1,305,750	12	1,305,762	0	79% $^3D_3$	79% $(3/2, 7/2)_3$	2
1,306,305(21)	−12	1,306,295	10	1,306,319	−14	69% $^3G_4$	96% $(3/2, 5/2)_4$	3
1,310,147(22)	10	1,310,110	37	1,310,158	−11	56% $^3G_3$	81% $(3/2, 5/2)_3$	2
1,311,707(30)	−24	1,311,730	−23	1,311,755	−48	50% $^3F_4$	95% $(3/2, 7/2)_4$	2
1,316,205(19)	15	…	…	1,316,758	−553	58% $^3F_2$	49% $(3/2, 7/2)_2$	2
1,323,654(24)	17	1,323,715	−61	1,323,657	−3	28% $^3F_3$	86% $(1/2, 5/2)_3$	3
1,324,670(30)	−42	1,324,680	−10	1,324,715	−45	38% $^1F_3$	83% $(1/2, 7/2)_3$	1
1,324,844(22)	46	1,324,885	−41	1,324,876	−32	30% $^1G_4$	93% $(1/2, 7/2)_4$	3
1,329,872(19)	−20	1,326,700?	3172	1,331,244	−1372	55% $^1D_2$	89% $(1/2, 5/2)_2$	2

Notes.
^{a} Key to references for the energy level values: O'D12—O'Dwyer et al. (2012), S76—Swartz et al. (1976), TW—this work.
^{b} Residual (obs.-calc.) of the parametric least-squares fit with Cowan's codes.
^{c} Percentages of the leading components in the eigenvector of each level in LS and JJ coupling. In LS coupling, the leading components of the 1,323,654, 1,324,670, and 1,324,844 cm^{-1} levels correspond to the second term of the eigenvector composition.
^{d} Number of observed lines determining the level value in the least-squares optimization procedure.
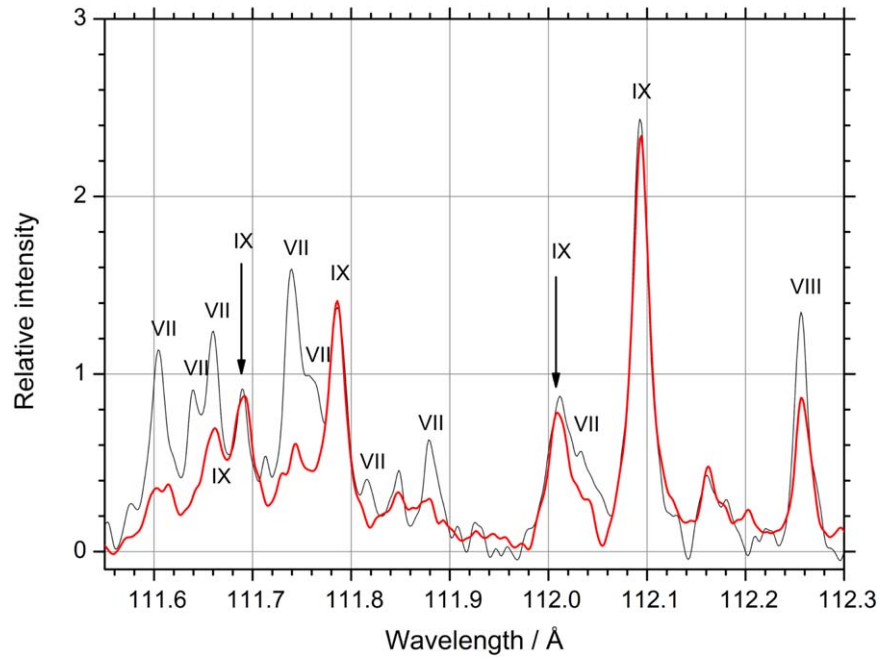
Figure 5. Two iron spectra correspond to hot (red) and cold (black) excitation conditions. The lines are marked by the symbols: VII—Fe VII, VIII—Fe VIII, and IX—Fe IX. Lines due to the three iron species are distinguished by their relative intensities in the two spectra. Arrows indicate the Fe IX lines at 111.692 and 112.011 Å.

Figure 6. The iron spectrum in the 133.8–134.3 Å range taken in the cold (black) and hot (red) modes of the spark operations (see Figure 5).

3.2. The $3p^53d$–$3p^43d^2$ Transitions

The $3p^43d^2$ comprises 109 fine-structure levels and the $3p^53d$–$3p^43d^2$ transition array gives rise to a large number of emission lines in the 150–270 Å region. Young (2009) was the first to identify lines from this array, using solar spectra obtained with Hinode/EIS. Further identifications from EIS spectra were suggested by Young & Landi (2009), Del Zanna (2009) and Del Zanna et al. (2014). Previous laboratory measurements of lines from the $3p^43d^2$ configuration have been made by Liang et al. (2009) and Beiersdorfer & Träbert (2018).

The wide wavelength coverage and high resolution of our spectra have enabled us to make many new line identifications from the $3p^53d$–$3p^43d^2$ and these are summarized in Table 3. Updated level energies are provided in Table 4. In total, 81 lines in the range 151–200 Å were identified, and five of them are doubly classified, i.e., two Fe IX transitions are assigned to the same observed line (marked with "db" in Column 2 of Table 3). The iron ion spectrum in this region is rich in lines. Depending on excitation conditions in a spark, the lines of Fe VI to Fe XII can be present and they can blend, mask, or perturb the Fe IX lines. Even at the high current modes, the

Table 3
Wavelengths of the $3p^5 3d$–$3p^4 3d^2$ Transitions in Fe IX

						$3p^5 3d$			$3p^4 3d^2$			
λ (Å)	Char.[a]	I[b]	gA[c]	λ_{Ritz} (Å)[d]	o-c[e]	Term	J	E (cm^{-1})	Term[f]	J	E (cm^{-1})	λ_{prev} (Å)[g]
151.549		200	205	151.550(2)	−0.001	^1D	2	456,752.7	$(^3P)^1Da$	2	1,116,602	
152.910		80	73	152.909(2)	0.001	^3D	2	462,616.6	$(^3P)^1Da$	2	1,116,602	
158.756		50	48	158.759(3)	−0.003	^3P	0	405,772	$(^1D)^3Da$	1	1,035,659	
159.011		130	101	159.014(2)	−0.003	^3P	1	408,315.1	$(^1D)^3Da$	2	1,037,191	
160.377		80	39	160.379(2)	−0.002	^3P	2	413,669.2	$(^1D)^3Da$	2	1,037,191	
162.178		400	300	162.183(3)	−0.005	^3P	2	413,669.2	$(^1D)^3Da$	3	1,030,255	
162.720		60	33	162.723(2)	−0.003	^3P	1	408,315.1	$(^3P)^3Fa$	2	1,022,856	
165.439	?	130	790	165.439(5)	…	^1P	1	584,546	$(^3P)^1S$	0	1,188,998	
168.483		70	91	168.479(2)	0.004	^3F	3	429,310.9	$(^3P)^3Fa$	2	1,022,856	
168.610		140	88	168.610(2)	0.000	^3F	4	425,809.8	$(^3P)^3Fa$	3	1,018,894	
169.242		260	138	169.245(2)	−0.003	^3D	3	455,612.2	$(^3P)^1F$	3	1,046,472	
169.407		160	201	169.410(3)	−0.003	^3P	0	405,772	$(^1D)^3Pa$	1	996,057	
169.579	p	420	259	169.572(2)	0.007	^1D	2	456,752.7	$(^3P)^1F$	3	1,046,472	
169.614		1240	1263	169.611(2)	0.003	^3F	3	429,310.9	$(^3P)^3Fa$	3	1,018,894	169.605 BT18TW
169.773	bl(VII)	∼500	744	169.769(2)	0.004	^3F	2	433,818.8	$(^3P)^3Fa$	2	1,022,856	
169.914		1380	1776	169.910(2)	0.004	^3F	4	425,809.8	$(^3P)^3Fa$	4	1,014,356	169.900 BT18TW
170.116		600	383	170.117(3)	−0.001	^3P	1	408,315.1	$(^1D)^3Pa$	2	996,147	170.11 BT18TW
170.150	w	290	87	170.143(3)	0.007	^3P	1	408,315.1	$(^1D)^3Pa$	1	996,057	
170.889	?	550	292	170.889(4)	…	^3P	1	408,315.1	$(^1D)^3Pa$	0	993,490	
170.924	db	740	158	170.918(2)	0.006	^3F	2	433,818.8	$(^3P)^3Fa$	3	1,018,894	170.92 BT18TW
170.924	db	740	197	170.927(2)	−0.003	^3F	3	429,310.9	$(^3P)^3Fa$	4	1,014,356	170.92 BT18TW
171.279		450	137	171.275(2)	0.004	^3D	2	462,616.6	$(^3P)^1F$	3	1,046,472	171.26 BT18TW
171.681	bl(VII)	1030	1048	171.680(3)	0.001	^3P	2	413,669.2	$(^1D)^3Pa$	2	996,147	171.685 BT18TW
171.706	bl(VII)	940	522	171.707(3)	−0.001	^3P	2	413,669.2	$(^1D)^3Pa$	1	996,057	
171.948		170	111	171.946(2)	0.002	^3D	3	455,612.2	$(^1D)^3Da$	2	1,037,191	
172.219		920	1180	172.223(2)	−0.004	^1F	3	465,828.4	$(^3P)^1F$	3	1,046,472	172.16[i] BT18TW
172.285		100	96	172.284(2)	0.001	^1D	2	456,752.7	$(^1D)^3Da$	2	1,037,191	
172.482		390	44	172.486(3)	−0.004	^3P	2	413,669.2	$(^1D)^3Db$	1	993,425	
172.795		70	33	172.796(3)	−0.001	^3P	2	413,669.2	$(^1D)^3Db$	2	992,387	
173.258		200	180	173.255(3)	0.003	^3P	0	405,772	$(^3P)^3S$	1	982,956	
173.902		780	537	173.900(3)	0.002	^3D	1	460,616	$(^1D)^3Da$	1	1,035,659	173.902 BT18TW
174.024	db	1530	1578	174.020(3)	0.004	^3D	3	455,612.2	$(^1D)^3Da$	3	1,030,255	174.03 BT18TW
174.024	db	1530	359	174.022(4)	0.002	^3P	1	408,315.1	$(^3P)^3S$	1	982,956	174.03 BT18TW
174.043		1400	945	174.042(2)	0.001	^3D	2	462,616.6	$(^1D)^3Da$	2	1,037,191	174 03 BT18TW
175.020	db	530	121	175.022(3)	−0.002	^1D	2	456,752.7	$(^1D)^1Da$	2	1,028,110	
175.020	db	530	770	175.020(2)	0.000	^1F	3	465,828.4	$(^1D)^3Da$	2	1,037,191	
175.551		60	26	175.552(2)	−0.001	^3F	4	425,809.8	$(^1S)^1G$	4	995,441	
175.648	db	420	409	175.642(3)	0.006	^3D	3	455,612.2	$(^3P)^3Pa$	2	1,024,953	
175.648	db	420	186	175.658(4)	−0.010	^3P	2	413,669.2	$(^3P)^3S$	1	982,956	
175.712		300	201	175.718(3)	−0.006	^3D	1	460,616	$(^3P)^3Pa$	1	1,029,709	
175.774	?	240	155	175.774(5)	…	^3D	1	460,616	$(^1S)^1S$	0	1,029,528	
175.993		140	147	175.994(3)	−0.001	^1D	2	456,752.7	$(^3P)^3Pa$	2	1,024,953	
176.289		320	77	176.291(2)	−0.002	^3D	3	455,612.2	$(^3P)^3Fa$	2	1,022,856	
176.344	bl(VII)	510	433	176.338(3)	0.006	^3D	2	462,616.6	$(^3P)^3Pa$	1	1,029,709	
176.599	?bl(VII)	520	632	176.599(5)	…	^1D	2	456,752.7	$(^3P)^1P$	1	1,023,007	
176.646		70	148	176.646(2)	0.000	^1D	2	456,752.7	$(^3P)^3Fa$	2	1,022,856	
176.840		240	124	176.837(3)	0.003	^3D	2	462,616.6	$(^1D)^1Da$	2	1,028,110	
176.978		1210	1598	176.978(5)	…	^3F	4	425,809.8	$(^1D)^3Db$	3	990,852	176.959[h] YL 176.945[h] D14
177.173	bl(VII)	850	179	177.171(3)	0.002	^1F	3	465,828.4	$(^1D)^3Da$	3	1,030,255	

Table 3
(Continued)

λ (Å)	Char.[a]	I[b]	gA[c]	λ_Ritz (Å)[d]	o-c[e]	3p⁵3d			3p⁴3d²			λ_prev (Å)[g]	
						Term	J	E (cm⁻¹)	Term[f]	J	E (cm⁻¹)		
177.599		780	958	177.596(3)	0.003	^3F	3	429,310.9	$(^1D)^3Db$	2	992,387	177.594 YL	177.592 D14
177.845		300	234	177.847(3)	−0.002	^1F	3	465,828.4	$(^1D)^1Da$	2	1,028,110		
177.856	db	300	325	177.860(2)	−0.004	^3D	1	460,616	$(^3P)^3Fa$	2	1,022,856		
177.856	db	300	47	177.861(3)	−0.005	^3F	2	433,818.8	$(^1D)^3Pa$	1	996,057		
177.888		270	151	177.891(2)	−0.003	^1D	2	456,752.7	$(^3P)^3Fa$	3	1,018,894		
178.059	bl(XI)	760	606	178.065(3)	−0.006	^3D	3	455,612.2	$(^3P)^1Db$	2	1,017,204		
178.431		40	60	178.428(3)	0.003	^1D	2	456,752.7	$(^3P)^1Db$	2	1,017,204		
178.701		930	626	178.697(3)	0.004	^3F	2	433,818.8	$(^1D)^3Db$	1	993,425	178.699 YL	
178.848		80	379	178.851(3)	−0.003	^1F	3	465,828.4	$(^3P)^3Pa$	2	1,024,953		
178.972		810	492	178.973(2)	−0.001	^3D	3	455,612.2	$(^3P)^3Fa$	4	1,014,356	178.985 YL	
179.027		530	69	179.029(3)	−0.002	^3F	2	433,818.8	$(^1D)^3Db$	2	992,387		
179.753	bl(XI)	1110	319	179.767(3)	−0.014	^3D	2	462,616.6	$(^3P)^3Fa$	3	1,018,894		
181.367		320	460	181.364(3)	0.003	^1F	3	465,828.4	$(^3P)^1Db$	2	1,017,204		
182.161	bl(XI)	1370	350	182.172(3)	−0.011	^3F	4	425,809.8	$(^3P)^3Fb$	4	974,743	182.158 LYTW	182.146 D09
182.305	bl	870	161	182.306(3)	−0.001	^1F	3	465,828.4	$(^3P)^3Fa$	4	1,014,356		
182.919		760	217	182.928(2)	−0.009	^3F	3	429,310.9	$(^3P)^3Fb$	3	975,974		
184.442		300	56	184.449(2)	−0.007	^3F	2	433,818.8	$(^3P)^3Fb$	3	975,974		
185.244	p(VIII)	650	144	185.244(3)	0.000	^3D	3	455,612.2	$(^1S)^1G$	4	995,441		
185.978		450	219	185.978(3)	0.000	^3F	2	433,818.8	$(^3P)^3Fb$	2	971,516	185.994 YLTW	
187.950		480	1461	187.950(3)	0.000	^1P	1	584,546	$(^3P)^1Da$	2	1,116,602	187.961 YLTW	
188.300	bl(XI)	1000	149	188.303(2)	−0.003	^3F	2	433,818.8	$(^1D)^1Fa$	3	964,878		
188.493		1920	1291	188.493(4)	…	^3F	4	425,809.8	$(^3P)^3Gb$	5	956,333	188.497 Y09	188.493 D09
188.678		240	79	188.680(3)	−0.002	^3F	4	425,809.8	$(^3P)^3Gb$	4	955,807	188.685 YL	
188.818		1160	745	188.817(3)	0.001	^1F	3	465,828.4	$(^1S)^1G$	4	995,441	188.823 LYTW	188.807 D09
189.577		400	130	189.578(3)	−0.001	^3F	3	429,310.9	$(^3P)^3Gb$	3	956,798	189.582 YL	
189.937		1820	958	189.935(3)	0.002	^3F	3	429,310.9	$(^3P)^3Gb$	4	955,807	189.941 Y09	189.935 D09
191.210		1290	544	191.212(3)	−0.002	^3F	2	433,818.8	$(^3P)^3Gb$	3	956,798	191.216 Y09	191.206 D09
192.182		200	28	192.174(2)	0.008	^3D	3	455,612.2	$(^3P)^3Fb$	3	975,974		
192.603		100	33	192.596(3)	0.007	^1D	2	456,752.7	$(^3P)^3Fb$	3	975,974		
192.633	bl(XI)	1040	374	192.630(3)	0.003	^3D	3	455,612.2	$(^3P)^3Fb$	4	974,743	192.632 YL	192.630 D14
194.796		940	302	194.796(2)	0.000	^3D	2	462,616.6	$(^3P)^3Fb$	3	975,974	194.806 YLTW	194.784[h] D09
195.733		670	209	195.733(3)	0.000	^3D	1	460,616	$(^3P)^3Fb$	2	971,516	195.743 YLTW	195.743 D09
196.356		300	35	196.361(2)	−0.005	^3D	3	455,612.2	$(^1D)^1Fa$	3	964,878		
196.499		190	39	196.496(3)	0.003	^1F	3	465,828.4	$(^3P)^3Fb$	4	974,743		
196.805		530	338	196.802(2)	0.003	^1D	2	456,752.7	$(^1D)^1Fa$	3	964,878	196.810 YLTW	196.803 D09
199.985		360	29	199.982(3)	0.003	^1D	2	456,752.7	$(^3P)^3Gb$	3	956,798	199.986 YL	
200.386		200	72	200.381(2)	0.005	^1F	3	465,828.4	$(^1D)^1Fa$	3	964,878		

Notes.

[a] Character of the observed line: db—intensity is shared by two transitions; bl—blended line (the blending species are given in parentheses where known): VII—Fe VII, VIII—Fe VIII, XI—Fe IX; ?—identification is uncertain; p—perturbed by a stronger nearby line (both the wavelength and intensity may be affected); w—wide line.

[b] Relative intensities are given on an arbitrary linear scale (see text).

[c] Weighted transition probability (g is the statistical weight of the upper level) in $10^9 \, s^{-1}$ unit.

[d] Wavelength derived from the final level energies (Ritz wavelength).

[e] Difference between the observed and Ritz wavelengths (blank for lines that solely determine the upper level).

[f] Designation is restricted to a term of the $3p^4$ sub-shell followed by a final term and a letter (a or b) distinguishing different terms of the $3d^2$ configuration in the case the final term is repeated. For full designation see Table 4.

[g] Previous measurements and identifications: BT18TW—measured by Beiersdorfer & Träbert (2018), identification of this work; D09—Del Zanna (2009); D14—Del Zanna et al. (2014); Y09—Young (2009); LYTW—line from Landi & Young (2009a), identification of this work; YL—Young & Landi (2009); YLTW—suggested as Fe IX lines by Young & Landi (2009), identification of this work.

[h] Lines are not fully resolved from, respectively, Fe VII 176.905 and 194.770 Å lines in EIS spectra.

[i] Line is blended with the O V line in the EBIT spectrum.

lines of lower stages of the ionization can be seen due to temporal and spatial inhomogeneity of the spark plasma. The spectra taken at the peak currents 50–100 kA were used for the Fe IX line measurements. The wavelengths were obtained from the spectra recordings on the photographic plates, while the intensities were taken from the imaging plates, where possible.

About 15 Fe IX lines have wavelengths close to known Fe VI–VIII lines (Azarov et al. 1996; Kramida et al. 2022; Ramonas & Ryabtsev 1980) or to the unidentified cold lines that are seen with high intensity in the spectra taken with lower peak currents. It was estimated, after a study of the behavior of the line intensities of these ion species on the peak current, that in

Table 4
Energy Levels of the $3p^4 3d^2$ Configuration of Fe IX Higher Than 930,000 cm^{-1}

E (cm^{-1})[a]	o-c[b]	J	Composition[c]			N[d]
931158#		1	61% (^3P)^3Da [$3p^4$(^3P)$3d^2$(^3F)^3D]	20% (^1D)^3Da	9% (^2S)$^3D^*$	
934730#		2	56% (^3P)^3Da [$3p^4$(^3P)$3d^2$(^3F)^3D]	18% (^1D)^3Da	8% (^2S)$^3D^*$	
934973#		1	74% (^3P)^3P [$3p^4$(^3P)$3d^2$(^1S)^3P]	12% (^3P)^3Pa	6% (^3P)^3Pb	
937428#		5	96% (^1D)^1H [$3p^4$(^1D)$3d^2$(^1G)^1H]	6% (^1D)^3G	1% (^3P)^3H	
937854#		0	73% (^3P)^3P [$3p^4$(^3P)$3d^2$(^1S)^3P]	12% (^3P)^3Pa	6% (^3P)^3Pb	
939790#		3	56% (^3P)^3Da [$3p^4$(^3P)$3d^2$(^3F)^3D]	20% (^1D)^3Da	8% (^2S)$^3D^*$	
943984#		2	55% (^1D)^3Fb [$3p^4$(^1D)$3d^2$(^3P)^3F]	28% (^1S)^3F	5% (^1D)^3Fa	
946522#		3	45% (^1D)^3Fb [$3p^4$(^1D)$3d^2$(^3P)^3F]	28% (^1S)^3F	6% (^1D)^3Fa	
949555#		4	44% (^1D)^3Fb [$3p^4$(^1D)$3d^2$(^3P)^3F]	38% (^1S)^3F	6% (^1D)^3Fa	
955807(9)	−279	4	37% (^3P)^3Gb [$3p^4$(^3P)$3d^2$(^1G)^3G]	32% (^1D)^3G	23% (^3P)^3Ga	2
956333(11)	13	5	41% (^3P)^3Gb [$3p^4$(^3P)$3d^2$(^1G)^3G]	33% (^1D)^3G	22% (^3P)^3Ga	1
956798(3)	−395	3	25% (^3P)^3Gb [$3p^4$(^3P)$3d^2$(^1G)^3G]	25% (^1D)^1Fa	23% (^1D)^3G	3
964878(10)	−102	3	64% (^1D)^1Fa [$3p^4$(^1D)$3d^2$(^1G)^1F]	14% (^3P)^3Gb	9% (^1D)^3G	4
971516(8)	−42	2	41% (^3P)^3Fb [$3p^4$(^3P)$3d^2$(^1G)^3F]	38% (^1D)^3Fa	15% (^1S)^3F	2
974743(11)	−78	4	37% (^3P)^3Fb [$3p^4$(^3P)$3d^2$(^1G)^3F]	33% (^1D)^3Fa	12% (^1S)^3F	3
975974(12)	283	3	39% (^3P)^3Fb [$3p^4$(^3P)$3d^2$(^1G)^3F]	33% (^1D)^3Fa	12% (^1S)^3F	5
982218#		0	55% (^1S)^3P [$3p^4$(^1S)$3d^2$(^3P)^3P]	40% (^1D)^3Pb	2% (^1D)^3Pa	
982956(12)	−179	1	79% (^3P)^3S [$3p^4$(^3P)$3d^2$(^3P)^3S]	13% (^1S)^3P	2% (^2P)^3S	3
983770#		1	47% (^1S)^3P [$3p^4$(^1S)$3d^2$(^3P)^3P]	33% (^1D)^3Pb	9% (^3P)^3S	
983927#		2	32% (^1D)^1D [$3p^4$(^1D)$3d^2$(^1S)^1D]	23% (^1S)^3P	13% (^1S)^1D	
987829#		2	38% (^1S)^3P [$3p^4$(^1S)$3d^2$(^3P)^3P]	17% (^1D)^1D	17% (^1D)^3Pb	
990852(13)	843	3	47% (^1D)^3Db [$3p^4$(^1D)$3d^2$(^3P)^3D]	14% (^3P)^3Db	13% (^3P)^3Da	1
991610#		4	58% (^1D)^1Ga [$3p^4$(^1D)$3d^2$(^1G)^1G]	26% (^1S)^1G	11% (^3P)^1G	
992387(9)	486	2	38% (^1D)^3Db [$3p^4$(^1D)$3d^2$(^3P)^3D]	13% (^3P)^3Db	12% (^3P)^3Da	3
993425(13)	−102	1	41% (^1D)^3Db [$3p^4$(^1D)$3d^2$(^3P)^3D]	14% (^3P)^3Db	12% (^3P)^3Da	2
993490(14)	125	0	48% (^1D)^3Pa [$3p^4$(^1D)$3d^2$(^3F)^3P]	35% (^3P)^3Pb	10% (^1S)^3P	1
995441(7)	−254	4	51% (^1S)^1G [$3p^4$(^1S)$3d^2$(^1G)^1G]	25% (^3P)^1G	10% (^1D)^1Ga	3
996057(10)	732	1	41% (^1D)^3Pa [$3p^4$(^1D)$3d^2$(^3F)^3P]	31% (^3P)^3Pb	10% (^1S)^3P	4
996147(10)	−497	2	38% (^1D)^3Pa [$3p^4$(^1D)$3d^2$(^3F)^3P]	35% (^3P)^3Pb	15% (^1S)^3P	2
1014356(8)	172	4	48% (^3P)^3Fa [$3p^4$(^3P)$3d^2$(^3F)^3F]	24% (^1S)^3F	11% (^3P)^3F	4
1017204(11)	245	2	32% (^3P)^1Db [$3p^4$(^3P)$3d^2$(^3P)^1D]	18% (^1D)^1Db	15% (^1D)^1D	3
1018894(9)	204	3	44% (^3P)^3Fa [$3p^4$(^3P)$3d^2$(^3F)^3F]	23% (^1S)^3F	11% (^3P)^3F	5
1022856(7)	582	2	27% (^3P)^3Fa [$3p^4$(^3P)$3d^2$(^3F)^3F]	15% (^1S)^3F	7% (^1D)^1Da	6
1023007(13)?	−220	1	42% (^3P)^1P [$3p^4$(^3P)$3d^2$(^3P)^1P]	25% (^1D)^1P	9% (^3P)^3Pa	1
1023390#		0	50% (^1S)^1S [$3p^4$(^1S)$3d^2$(^1S)^1S]	14% (^3P)^3Pa	13% (^1D)^1S	
1024953(10)	−331	2	31% (^3P)^3Pa [$3p^4$(^3P)$3d^2$(^3P)^3P]	18% (^1D)^3Pb	12% (^3P)^3P	3
1028110(9)	−388	2	22% (^1D)^1Da [$3p^4$(^1D)$3d^2$(^1G)^1D]	15% (^2S)$^1D^*$	12% (^3P)^3Fa	3
1029528(13)?	−1504	0	23% (^1S)^1S [$3p^4$(^1S)$3d^2$(^1S)^1S]	21% (^3P)^3Pa	15% (^3P)^3P	1
1029709(17)	317	1	23% (^3P)^3Pa [$3p^4$(^3P)$3d^2$(^3P)^3P]	14% (^3P)^1P	10% (^1S)^3P	2
1030255(15)	−1093	3	34% (^1D)^3Da [$3p^4$(^1D)$3d^2$(^3F)^3D]	20% (^3P)^3Db	17% (^3P)^3Da	2
1035659(12)	−1451	1	36% (^1D)^3Da [$3p^4$(^1D)$3d^2$(^3F)^3D]	24% (^3P)^3Db	18% (^3P)^3Da	2
1037191(7)	197	2	31% (^1D)^3Da [$3p^4$(^1D)$3d^2$(^3F)^3D]	21% (^3P)^3Db	17% (^3P)^3Da	6
1046472(10)	1158	3	54% (^3P)^1F [$3p^4$(^3P)$3d^2$(^3F)^1F]	19% (^1D)^1Fb	19% (^2P)$^3D^{**}$	4
1116602(8)	8	2	54% (^3P)^1Da [$3p^4$(^3P)$3d^2$(^3F)^1D]	24% (^1D)^1Da	7% (^3P)^1Db	3
1188998(15)?	136	0	63% (^3P)^1S [$3p^4$(^3P)$3d^2$(^3P)^1S]	17% (^1D)^1S	12% (^1S)^1S	1

Notes.
[a] # calculated value for the level; ? questionable levels not included in the fitting.
[b] Residual (obs.–calc.) of the parametric least-squares fit with Cowan's codes in cm^{-1}.
[c] LS composition of the level eigenvector. The $3p^4$ configuration terms and the final terms are listed. The letters after the final terms distinguish different terms of the $3d^2$ configuration. Full descriptions for the first component are shown in square brackets. * (^2S)^1D and (^2S)^3D terms belong to the $3s3p^63d$ configuration; ** (^2P)^3D stands for $3p^5$(^2P)$4p$(^2P)^3D.
[d] Number of observed lines determining the level value in the least-squares optimization procedure.

most cases their influence on the Fe IX lines is negligible. We found and marked in Table 3 only six lines that could have a contribution to their intensities from cold lines (marked with bl(VII) or bl(VIII) in Table 3)

The relative intensities are given on a linear scale without accounting for the wavelength dependence of the spectrograph and imaging plate effectivities. The resonance Fe IX line at 171.073 Å has in our spectrum the intensity 6000 on this scale. The scale is not directly connected to that of the $3p^53d$–$3p^54f$ transitions because the spectra were taken on different recording media and with different excitation in the vacuum spark. According to rough estimates, the scales can be different by a factor of two.

Table 4 lists the 45 levels in the upper level range of the $3p^4 3d^2$ configuration (energies above 930,000 cm^{-1}). The 81 lines identified in the present work yield energies for 30 of these levels. Three of the level energies are uncertain (marked with a ? in the table) as they are based on a single questionable line identification. The second column of the table compares the observed energies with the energies obtained from Cowan's code using parametric calculations. The remaining 15 levels in Table 4 are listed for completeness and the energies are those from Cowan's code. The values should be valuable for future efforts to identify Fe IX transitions. Table 4 also gives the first three components of each level's eigenvector. The first component of the eigenvector together with the energy level value was used as a label for the transitions in Table 3. A difficulty in the level designation should be pointed out. The $3p^4 3d^2$ configuration consists of two sub-shells with more than one electron. For unambiguous level designation all intermediate quantum numbers should be given $3p^4 (L'S') 3d^2 (L''S'') LS$. Shorthand designation by the $L'S'$ numbers together with the final LS is adopted in the Cowan code resulting in an ambiguity of the repeated final LS numbers belonging to the same $L'S'$ but to different $L''S''$. The letters a or b are added to distinguish between such cases. The full descriptions for the first components of the eigenvectors are shown in Table 4 in square brackets.

The energy parameters after the least-squares fitting of the calculated to the experimental energy levels are shown in Table 5. The electrostatic parameters for the configurations with unknown levels as well as the configuration interaction parameters were scaled by a factor of 0.85 with respect to the corresponding Hartree–Fock with relativistic corrections (HFR) values (see p. 464 of Cowan 1981). Only a parameter of interaction between the $3s^2 3p^4 3d^2$ and $3s 3p^6 3d$ configurations was fitted for better description of the levels with mixed eigenvectors. The spin–orbit parameters were not scaled, and all of them are omitted from Table 5. The average energies of these configurations were scaled so that their differences from those of the known configurations were approximately the same as in the HFR calculations. The parameters of Table 5 were used for the calculations of the energy levels and transition probabilities of the Fe IX spectrum. The branching ratios for the intensities of the lines from a particular level generally follow the calculated transition probabilities with three exceptions. The intercombination line $^1D_2$–$(^3P)^3Gb$ ($J = 3$) at 199.985 Å is too intense and two other intercombination lines $^1D_2$–$(^3P)^3Fa$ ($J = 2$) and $^1F_3$–$(^3P)^3Pa$ ($J = 2$) at, respectively 176.646 and 178.848 Å are too weak in their transition arrays.

Most of the lines with gA greater than 5×10^{10} s^{-1} were identified, with the exception of the decays from the $(^3P)^3Da$ term. The three $^3P_{J-1}$–$(^3P)^3D_J a$ ($J = 3, 2, 1$) transitions have $gA = 5.2 \times 10^{11}$, 2.9×10^{11}, and 1.4×10^{11} s^{-1} and calculated wavelengths 190.07, 189.96, and 190.34 Å, respectively. The lines may be blended with lines at 190.037 Å (Fe X), 189.937 Å (Fe IX), and 190.296 Å (Fe VI).

Finally, we give a few remarks about previous measurements and identifications of the Fe IX lines.

Several laboratory studies of Fe IX were undertaken with the aid of the Heidelberg (Liang et al. 2009) or the Lawrence Livermore National Laboratory (Beiersdorfer & Lepson 2012; Beiersdorfer & Träbert 2018) EBIT. The observed spectra showed the evolution of each ionic stage from Fe^{5+} to at least Fe^{15+} as a function of the electron energy, allowing the authors to distinguish the emission lines from the neighboring ion charge states.

The spectra of Liang et al. (2009) were recorded in the 125–265 Å range with 0.5–0.8 Å resolution. Four lines (188.5, 189.9, 191.2, and 197.9 Å) were suggested as belonging to Fe IX, and these were independently identified by Young (2009) from EIS spectra. The first three lines belong to the $3p^5 3d \ ^3F$–$3p^4 3d^2$ $(^3P)^3G$ multiplet, and the fourth is the $3p^5 3d \ ^1P_1$–$3p^5 4p \ ^1S_0$ transition.

Beiersdorfer & Lepson (2012) measured with a resolution of about 0.3 Å a dozen spectral features in the 170–200 Å range, some of which could be attributed to Fe IX based on ionization energy and wavelength coincidences with a CHIANTI spectral model. Version 7.0 (Landi et al. 2012) of CHIANTI was used, which mostly had only theoretical wavelengths for the lines in this wavelength range and so definitive new identifications could not be made. The authors did provide supporting data for some of the identifications of Young (2009) and Young & Landi (2009), however.

Beiersdorfer & Träbert (2018) (hereafter BT18) studied emission in the wavelength region 165–175 Å from various species excited in an EBIT, including Fe IX. The spectral resolution was 3000 and wavelengths were measured with uncertainties of 10–20 mÅ. The spectrum produced by a beam energy 300 eV yielded lines mainly due to Fe IX and Fe X. The authors modeled the Fe IX emission by employing atomic data computed with the relativistic Multi-Reference Møller–Plesset (MR-MP) perturbation theory (Vilkas et al. 1999) and the Flexible Atomic Code (FAC; Gu 2008). By comparing their predicted spectra with the EBIT measurements, BT18 were able to match features in their modeled spectra to features in the EBIT spectrum based on proximity in wavelength and intensity. Some of the lines were blended with other species.

The MR-MP method has previously been shown to yield level energies with spectroscopic accuracy. For example, the $n = 3$ levels of Fe XIII (Vilkas & Ishikawa 2004) are reproduced to around 0.01%. However, earlier works did not address complex configurations of the form $3p^k 3d^m$ ($k < 6$, $m > 1$). Recently, Santana et al. (2020) performed MR-MP calculations for Fe VIII and derived $3p^5 3d^2$ energies with accuracies up to 0.8%, which is not high enough for classifying unidentified lines. Although not investigated by BT18, such uncertainties may also apply to their calculations for the $3p^4 3d^2$ configuration of Fe IX.

BT18 did not publish their Fe IX atomic data and so it is not possible to compare radiative decay rates with the present or earlier calculations. However, they do comment that the $3p^4 3d^2$ $(^1D)^3D_3 a$ level (using our level notation) has its strongest decay to $3p^5 3d \ ^3F_3$ whereas the CHIANTI 8 atomic model has the strongest decay to $3p^5 3d \ ^3D_3$. The CHIANTI 8 model decay rates are from Del Zanna et al. (2014) and are comparable to the present decay rates. We compared with the calculations of Storey et al. (2002) and Tayal & Zatsarinny (2015), and these both confirmed that the strongest decay is to the $^3D_3$ level. This particular discrepancy affects the identification of the lines at 167.478 and 174.03 Å measured by BT18, as discussed below.

Of the 16 Fe IX lines identified in Table 5 of BT18, seven are present in our spectra and we also assign them to Fe IX. The BT18 line at 172.16 Å was blended with O V in their spectrum but this is not the case in our spectra. BT18 noted that lines at 170.92 and 173.90 Å could be due to Fe IX. Both lines are present in our spectra with Fe IX properties. All nine of

Table 5
HFR and Least-square-fitted (LSF) Parameter Values (cm^{-1}) with Their Uncertainties (Unc.) in Fe IX

Configuration	Parameter	LSF	Unc.[a]	HFR[b]	LSF/HFR[c]
Even configurations					
$3s^23p^6$	E_{av}	31,763	571	30,744	1.032
$3s^23p^54p$	E_{av}	1,054,771	f	1,084,771	0.971
$3s^23p^55p$	E_{av}	1,406,545	f	1,436,545	0.978
$3s^23p^56p$	E_{av}	1,573,258	f	1,603,258	0.980
$3s^23p^54f$	E_{av}	1,310,977	165	1,340,635	0.977
	$\zeta(3p)$	1,034,0	330	1,013,0	1.021
	$\zeta(4f)$	21	f	21	1.000
	$F^2(3p, 4f)$	36,124	2265	38,697	0.933
	$G^2(3p, 4f)$	18,411	1313	21,281	0.865
	$G^4(3p, 4f)$	13,303	4016	14,048	0.947
$3s^23p^55f$	E_{av}	1,520,529	f	1,550,529	0.980
$3s^23p^56f$	E_{av}	1,634,436	f	1,664,436	0.981
$3s^23p^43d^2$	E_{av}	906,997	463	938,864	0.964
	$F^2(3p, 3p)$	127,124	3697	132,065	0.963
	$\alpha(3p)$	199	223	…	…
	$F^2(3d, 3d)$	105,070	3063	131,852	0.797
	$F^4(3d, 3d)$	63,148	4848	84,189	0.750
	$\zeta(3p)$	10,012	482	9698	1.032
	$\zeta(3d)$	753	169	798	0.944
	$F^2(3p, 3d)$	117,806	1170	128,513	0.917
	$G^1(3p, 3d)$	128,628	598	153,097	0.840
	$G^3(3p, 3d)$	79,137	2044	97,017	0.816
$3s3p^63d$	E_{av}	800,263	977	829,259	0.962
	$\zeta(3d)$	755	169	800	0.944
	$G^2(3s, 3d)$	120,637	2520	119,177	1.012
$3s3p^64s$	E_{av}	1,314,892	f	1,344,892	0.976
	$G^0(3s, 4s)$	8928	f	10,505	0.850
$3s^23p^43d4s$	E_{av}	1,406,139	f	1,436,139	0.978
$3s^23p^44s2$	E_{av}	1,975,829	f	2,005,829	0.984
$3s^23p^44s4d$	E_{av}	2,220,346	f	2,250,346	0.986
	$R^1(3s, 3d; 3p, 3p)$[d]	145,004	897	160,894	0.901
	σ[e]	555	…	…	…
Odd configurations					
$3s^23p^53d$	E_{av}	448,456	16	477,759	0.932
	$\zeta(3p)$	9921	48	9686	1.024
	$\zeta(3d)$	784	18	798	0.982
	$F^1(3p, 3d)$	4862	121	0	…
	$F^2(3p, 3d)$	115,238	143	128,765	0.895
	$G^1(3p, 3d)$	129,360	47	153,302	0.844
	$G^2(3p, 3d)$	5252	245	0	…
	$G^3(3p, 3d)$	84,578	258	97,191	0.870
$3s^23p^54d$	E_{av}	1,199,786	38	1,233,059	0.971
	$\zeta(3p)$	10,616	50	10,082	1.053
	$\zeta(4d)$	220	f	220	1.000
	$F^2(3p, 4d)$	31,127	f	36,620	0.850
	$G^1(3p, 4d)$	8573	f	10,085	0.850
	$G^3(3p, 4d)$	8520	f	10,023	0.850
$3s^23p^55d$	E_{av}	1,469,453	f	1,502,453	0.977
$3s^23p^56d$	E_{av}	1,605,451	f	1,638,451	0.979
$3s^23p^54s$	E_{av}	954,374	39	985,623	0.966
	$\zeta(3p)$	10,307	58	10,077	1.023
	$G^1(3p, 4s)$	11,655	f	13,711	0.850
$3s^23p^55s$	E_{av}	1,362,553	38	1,392,738	0.977
	$\zeta(3p)$	10,292	49	10,138	1.015
	$G^1(3p, 5s)$	3940	f	4636	0.850
$3s3p^64p$	E_{av}	1,408,803	f	1,440,803	0.977
$3s3p^64f$	E_{av}	1,665,072	f	1,697,072	0.980
	σ[e]	51			

Notes.

[a] f—fixed parameter.

[b] Average energies are adjusted so that the energy of the ground level $3s^23p^6$ $^1S_0$ is zero in the calculation of the even configuration matrix with all electrostatic parameters scaled by 0.85 factor.

[c] Electrostatic parameters of the configurations, as well as interaction parameters not listed in the table, are scaled by a factor of 0.85 with respect to ab initio values; the spin–orbit parameters are not scaled.

[d] Parameter of interaction between the $3s^23p^43d^2$ and $3s3p^63d$ configurations.
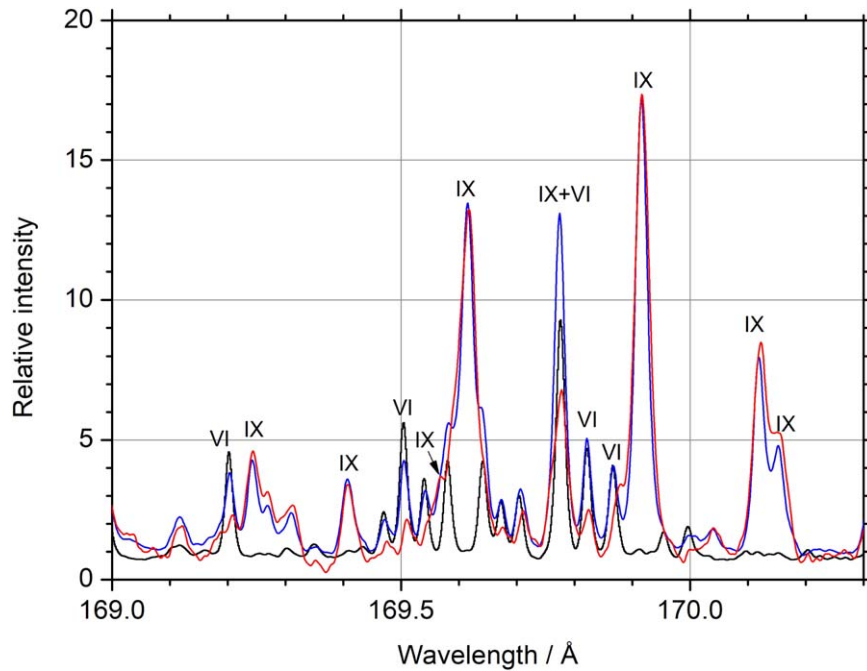
[e] rms deviation of the fitting.

Figure 7. The iron spectrum in the range 169.0–170.3 Å taken at three modes of the spark operation: cold—black, *intermediate*—blue, and hot—red. The lines are marked by the symbols: VI—Fe VI (only prominent lines), and IX—Fe IX. The relative intensities in arbitrary units are scaled so that the Fe IX lines have approximately the same intensities in the intermediate and hot spectra, whereas the Fe VI lines have approximately the same intensities in the cold and intermediate spectra.

the BT18 measured wavelengths are given in the λ_{pred} column of Table 3.

The higher resolution of our spectra allows us to resolve the 170.11 Å line of BT18 into two lines at 170.116 and 170.150 Å (see Figure 7). The line at 174.03 Å is also resolved into two lines at 174.024 and 174.043 Å, and the former is a double blend of two Fe IX transitions (Table 3).

Of the seven BT18 lines for which they assigned identifications, we confirm only one: the $3p^53d\,^3D_3$–$3p^43d^2\,(^1D)^3D_3a$ transition at 174.03 Å. This is the strongest of a pair of transitions that are double-blended in our spectra at 174.024 Å (Table 3). Both identifications are supported by multiple Ritz combinations. Although we agree with the BT18 identification, we note that the BT18 atomic model predicted this transition to be the weakest of all the decays from the $3p^43d^{23}D_3a$ level, yet the measured line is quite strong in their spectra. This is a consequence of the problem with this level noted earlier.

Of the remaining six lines for which identifications disagree, we find two belong to the set of three $3p^53d\,^3F_J$–$3p^43d^2$ $(^3P)^3F_Ja$ transitions. The BT18 wavelengths 169.605 and 169.900 Å match our wavelengths 169.614 and 169.914 Å, corresponding to the transitions with $J = 3$ and $J = 4$, respectively. We identify the $J = 2$ transition with a line at 169.773 Å (see discussion below). Each identification is supported by between four and six Ritz combinations. The 2–3 and 3–4 members of the same multiplet comprise the 170.92 Å feature in the BT18 spectrum, with Ritz wavelengths of 170.918 and 170.927 Å, respectively. The other Ritz combinations within the 165–175 Å range are at 168.483 and 168.610 Å (Table 3) and lie close to a strong Fe VIII line in the BT18 spectrum and were not reported by BT18.

The identification of the 169.773 Å line warrants further discussion as BT18 stated that this line must come from a spectrum lower than Fe IX. Figure 7 shows the spectra in the region of this line taken at different excitation conditions in the

spark. The intensities in the spectra are scaled so that their comparison can help in the attribution of the lines to different ions. The 169.773 Å line is clearly blended with a strong Fe VI line (Azarov et al. 1996). But a comparison of the changes in its intensity with those of the other Fe VI and Fe IX lines clearly shows that the main contribution to the intensity of this line in hot conditions comes from Fe IX. The identification is supported by the observation of an additional five Ritz lines in our spectra.

Two more of the six BT18 lines for which we have different identifications are 170.11 and 171.685 Å. These are the two strongest decays of the $(^1D)^3Pa$ $(J = 2)$ level to $3p^53d\,^3P_1$ and $^3P_2$, respectively, that we measure at 170.116 and 171.681 Å. Three additional Ritz combinations outside of the BT18 wavelength range are reported in Table 3. The remaining two BT18 lines are at 171.26 and 172.16 Å and we identify them with decays from the $(^3P)^1F_3$ level. Our wavelengths are 171.279 Å and 172.219 Å and they correspond to decays to the $3p^53d\,^3D_2$ and $^1F_3$ levels, respectively. Note the latter is blended with O V in the BT18 spectrum hence the wavelength discrepancy. A third decay to the $^1D_2$ level can be identified as an enhanced wing to the strong 169.614 Å line, as indicated in Figure 7.

BT18 listed two strong transitions at 167.478 and 167.654 Å as blends of Fe IX with Fe VIII. The former identification was made on account of the BT18 atomic model predicting the strongest transition from the $3p^43d^2\,(^1D)^3D_3a$ level near this wavelength. As noted earlier this prediction is at odds with other atomic calculations, and our spectra do not suggest a contribution from Fe IX. A similar problem may affect the BT18 identification of the 167.654 Å line. That is, if their atomic model predicts the $3p^53d\,^3F_2$–$3p^43d^2\,^3D_2a$ to be the strongest decay, then this disagrees with our atomic calculations and those in CHIANTI. As with the 167.478 Å line, we do not find evidence of an Fe IX contribution.

The remaining seven Fe IX lines listed by BT18 that are not found in our spectra were weak in their spectrum (intensities $\leqslant 0.1$ on the BT18 scale). They could belong to other stages of ionization, but the different excitation conditions in the EBIT compared to our spark spectrum could also be responsible for the differences. The EBIT plasma has a lower density that is more typical of the solar corona.

A breakthrough in the analyses of the Fe IX $3p^5 3d$–$3p^4 3d^2$ lines in the Sun's spectrum came from observations by Hinode/EIS. The two wavelength bands 170–212 and 246–292 Å are observed with a spectral resolution of around 0.06 Å. Imaging capability is critical to discriminating between neighboring ionization stages, as demonstrated by Young (2009) who compared images of coronal loop structures in lines of Fe VIII through Fe X.

Landi & Young (2009a) created an atlas of the Sun's spectral lines of ions formed between 10^5 K and 10^6 K from a bright point related to the footpoint region of a coronal loop. The intensities of cold lines were enhanced over normal values in this atlas. It permitted to make the first identification of three lines from the $3p^5 3d$–$3p^4 3d^2$ transitions, namely, the main lines from the $3p^5 3d\,^3F$–$3p^4 3d^2\,(^3P)^3G$ multiplet (Young 2009) mentioned above. In an extension of this result, Young & Landi (2009) found the Ritz combinations for the $3p^4 3d^2\,(^3P)^3G_{4,3}$ levels, thus confirming their identifications. Three lines (176.959, 177.594, and 199.986 Å) were added as the transitions to the $3p^5 3d\,^3F_{3,4}$ levels from the $3p^4 3d^2\,(^1D)^3D_{3,2}$ levels. It should be noted that the first line in the EIS spectrum is not fully resolved from the Fe VII 176.905 Å line. The wavelength of this line is 176.978 Å from our fully resolved spectrum. Two other lines at 178.699 and 178.985 A were tentatively suggested as the $3p^5 3d\,^3F_2$–$3p^4 3d^2$ $(^1D)^3D_1$ and $3p^5 3d\,^3D_3$–$3p^4 3d^2\,(^3P)^3Fa$ $(J=4)$ transitions, respectively. We have confirmed these suggestions. In summary, ten lines in the $3p^5 3d$–$3p^4 3d^2$ array of Fe IX were identified with specific $3p^4 3d^2$ levels.

Young & Landi (2009) published a list of seven additional observed lines that were suggested as being due to Fe IX based on image morphology, but for which transition identifications could not be assigned. We have identified all but one of these lines and marked them with YLTW in Table 3. On a basis of our laboratory spectrum, we have identified three additional lines in the Landi & Young (2009a) atlas. The 182.158, 188.823, and 194.806 Å EIS lines are identified, respectively, with $3p^3 3d\,^3F_4$–$3p^4 3d^2\,(^3P)^3Fb$ $(J=4)$, $3p^3 3d\,^1F_3$–$3p^4 3d^2\,(^1S)^1G_4$, and $3p^3 3d\,^3D_2$–$3p^4 3d^2$ $(^3P)^3Fb$ $(J=3)$ transitions. The latter is not fully resolved from the Fe VII 194.770 Å line in the EIS spectrum, and our laboratory wavelength is 194.796 Å. Note that the wavelengths of all the EIS Fe IX lines from the Landi & Young (2009a) atlas listed in Table 3 are corrected for the redshift with velocity 16 km s^{-1} as suggested by Young & Landi (2009).

Del Zanna (2009) published a spectral atlas from a coronal loop rooted in a sunspot that also exhibited strongly enhanced cool emission lines. Del Zanna confirmed the Young (2009) identifications of the three main lines of the $3p^5 3d\,^3F$–$3p^4 3d^2$ $(^3P)^3G$ multiplet and Del Zanna tentatively identified three weak transitions from the $3p^4 3d^2$ configuration levels that we reject. However, the line list contains many other lines left unidentified or considered as blends that are also present in the Landi & Young (2009a) atlas and are identified in our laboratory spectrum. These lines are marked with D09 in Table 3. Their wavelengths were corrected for a redshift of 10 km s^{-1}.

Large-scale intermediate-coupling R-matrix scattering calculations for electron collisional excitation of Fe IX were performed by Del Zanna et al. (2014). The data were used to create a new atomic model for the ion, and intensities were computed and compared with observations. Good agreement with the known Fe IX lines in the EIS spectrum was obtained. Based on this agreement a few new weak Fe IX lines were tentatively identified (Del Zanna 2009). We confirmed the identification of one line at 192.630 Å as the $3p^5 3d\,^3D_3$–$3p^4 3d^2$ $(^3P)^3Fb$ $(J=4)$ transition. The identification of the 194.784 Å line was changed. The other suggested lines are absent in our laboratory spectra, perhaps because of different excitation conditions in the Sun and our spark spectra or they belong to Fe VII (Ekberg 1981; Kramida et al. 2022).

The $3p^5 3d$–$3p^5 4p$ lines should be also located in the studied wavelength range. As mentioned above, a line at 197.862 Å in the EIS spectrum was identified as the $3p^5 3d\,^1P_1$–$3p^5 4p\,^1S_0$ transition by Young (2009). This identification was supported by the observation of two lines at 717.661 and 803.422 Å, corresponding to decays to the $3p^5 4s\,^1P_1$ and $^3P_1$ levels (Landi & Young 2009b). These lines were measured with the Solar Ultraviolet Measurements of Emitted Radiation (Wilhelm et al. 1995) instrument. The 197.862 Å line is very weak in our spectrum. We did not succeed in finding any other lines of the $3p^5 3d$–$3p^5 4p$ transitions, which possess smaller transition probabilities than the 197.862 Å line. Since only one upper level is known in the $3p^5 4p$ configuration, we considered this configuration as *unknown* in our calculations, scaling only its average energy by a predetermined factor (Table 5). In this approach, the calculated energy of the $3p^5 4p\,^1S_0$ level is lower than the experimental one by about 3900 cm^{-1}.

4. Conclusions

Using high-resolution laboratory spectra in the 110–200 Å range the analysis of energy levels and spectral lines of Fe IX was greatly extended. Many weak lines were added to the previous analyses of the $3p^5 3d$–$3p^5 4f$ transitions extending the number of identified lines to 25. Seventy-three lines of the $3p^5 3d$–$3p^4 3d^2$ transition array were identified, bringing the number of known lines in this transition array to 81. A number of lines assigned to Fe IX were identified in Hinode/EIS spectra. The data can be used for diagnostics of solar plasma and provide a benchmark for further development of atomic theory.

ORCID iDs

Alexander N. Ryabtsev ⓘ https://orcid.org/0000-0002-5321-5406
Peter R. Young ⓘ https://orcid.org/0000-0001-9034-2925

References

Alexander, E., Feldman, U., Fraenkel, B. S., & Hoory, S. 1965, Natur, 206, 176
Azarov, V. I., Kramida, A., & Vokhmentsev, M. Y. 2018, CoPhC, 225, 149
Azarov, V. I., Podobedova, L. I., & Ryabtsev, A. N. 1996, PhyS, 53, 398
Behring, W. E., Cohen, L., & Feldman, U. 1972, ApJ, 175, 493
Beiersdorfer, P., & Lepson, J. K. 2012, ApJS, 201, 28
Beiersdorfer, P., & Träbert, E. 2018, ApJ, 854, 114

Brown, C. M., Feldman, U., Seely, J. F., Korendyke, C. M., & Hara, H. 2008, ApJS, 176, 511

Cowan, R. D. 1981, The Theory of Atomic Structure and Spectra (Berkeley, CA: Univ. California Press)

Culhane, J. L., Harra, L. K., James, A. M., et al. 2007, SoPh, 243, 19

Del Zanna, G. 2009, A&A, 508, 501

Del Zanna, G. 2012, A&A, 546, A97

Del Zanna, G., & DeLuca, E. E. 2018, ApJ, 852, 52

Del Zanna, G., Dere, K. P., Young, P. R., & Landi, E. 2021, ApJ, 909, 38

Del Zanna, G., Storey, P. J., Badnell, N. R., & Mason, H. E. 2014, A&A, 565, A77

Delaboudinière, J. P., Artzner, G. E., Brunaud, J., et al. 1995, SoPh, 162, 291

Drake, J. J., Laming, J. M., & Widing, K. G. 1995, ApJ, 443, 393

Drake, J. J., Laming, J. M., & Widing, K. G. 1997, ApJ, 478, 403

Edlen, B., & Smitt, R. 1978, SoPh, 57, 329

Ekberg, J. O. 1981, PhyS, 23, 7

Engström, L. 1998, GFit, a Computer Program to Determine Peak Positions and Intensities in Experimental Spectra: Lund Reports on Atomic Physics LRAP-232,, Lund Univ.

Fawcett, B. C., Kononov, E. Y., Hayes, R. W., & Cowan, R. D. 1972, JPhB, 5, 1255

Feldman, U., Doschek, G. A., & Widing, K. G. 1978, ApJ, 219, 304

Foster, A. R., & Testa, P. 2011, ApJL, 740, L52

Gabriel, A. H., & Fawcett, B. C. 1965, Natur, 206, 390

Handy, B. N., Acton, L. W., Kankelborg, C. C., et al. 1999, SoPh, 187, 229

Gu, M. F. 2008, CaJPh, 86, 675

Howard, R. A., Moses, J. D., Vourlidas, A., et al. 2008, SSRv, 136, 67

Kramida, A. 2019, NIST Public Repository (A suite of atomic structure codes originally developed by R. D. Cowan adapted for Windows-based personal computers) (Gaithersburg, MD: National Institute of Standards and Technology),

Kramida, A., Ralchenko, Y., Reader, J. & NIST ASD Team 2021, NIST Atomic Spectra Database (ver. 5.9), [Online]. Available: https://physics.nist.gov/asd, National Institute ofStandards and Technology, Gaithersburg, MD

Kramida, A., Ryabtsev, A. N., & Young, P. R. 2022, ApJS, 258, 37

Kramida, A. E. 2011, CoPhC, 182, 419

Landi, E., Del Zanna, G., Young, P. R., Dere, K. P., & Mason, H. E. 2012, ApJ, 744, 99

Landi, E., & Young, P. R. 2009a, ApJ, 706, 1

Landi, E., & Young, P. R. 2009b, ApJ, 707, 1191

Lemen, J. R., Title, A. M., Akin, D. J., et al. 2012, SoPh, 275, 17

Lepson, J. K., Beiersdorfer, P., Brown, G. V., et al. 2002, ApJ, 578, 648

Liang, G. Y., Baumann, T. M., López-Urrutia, J. R. C., et al. 2009, ApJ, 696, 2275

Malinovsky, L., & Heroux, M. 1973, ApJ, 181, 1009

O'Dwyer, B., Del Zanna, G., Badnell, N. R., Mason, H. E., & Storey, P. J. 2012, A&A, 537, A22

Ramonas, A. A., & Ryabtsev, A. N. 1980, OptSp, 48, 348

Rochus, P., Auchère, F., Berghmans, D., et al. 2020, A&A, 642, A8

Ryabtsev, A. N. 2017, EPJWC, 132, 03043

Santana, J. A., Ishikawa, Y., & Beiersdorfer, P. 2020, ApJS, 247, 52

Storey, P. J., Zeippen, C. J., & Le Dourneuf, M. 2002, A&A, 394, 753

Svensson, L. Å., & Ekberg, J. O. 1969, Ark. Fys., 40, 145

Swartz, M., Kastner, S. O., Goldsmith, L., & Neupert, W. M. 1976, JOSA, 66, 240

Tayal, S. S., & Zatsarinny, O. 2015, ApJ, 812, 174

Vilkas, M. J., & Ishikawa, Y. 2004, PhRvA, 69, 062503

Vilkas, M. J., Ishikawa, Y., & Koc, K. 1999, PhRvA, 60, 2808

Wagner, W. J., & House, L. L. 1971, ApJ, 166, 683

Wilhelm, K., Curdt, W., Marsch, E., et al. 1995, SoPh, 162, 189

Woods, T. N., Eparvier, F. G., Hock, R., et al. 2012, SoPh, 275, 115

Young, P. R. 2009, ApJL, 691, L77

Young, P. R., Del Zanna, G., Mason, H. E., et al. 2007, PASJ, 59, S857

Young, P. R., Dere, K. P., Landi, E., Del Zanna, G., & Mason, H. E. 2016, JPhB, 49, 074009

Young, P. R., & Landi, E. 2009, ApJ, 707, 173

Young, P. R., Ryabtsev, A. N., & Landi, E. 2021, ApJ, 908, 104